Inorganic Chemistry

Article

pubs.acs.org/IC

Synthesis, Crystal Structure, and Magnetic Properties of the Coordination Polymer $[Fe(NCS)_2(1,2\text{-bis}(4\text{-pyridyl})\text{-ethylene})]_n$ Showing a Two Step Metamagnetic Transition

Susanne Wöhlert,[†] Mario Wriedt,[‡] Tomasz Fic,[§] Zbigniew Tomkowicz,[§] Wolfgang Haase,[∥] and Christian Näther*,[†]

[†]Institut für Anorganische Chemie, Christian-Albrechts-Universität zu Kiel, Max-Eyth-Strasse 2, D-24118 Kiel, Germany

[‡]Department of Chemistry, Texas A&M University, College Station, Texas 77843, United States

[§]Institute of Physics, Jagiellonian University, Reymonta 4, 30-059 Kraków, Poland

[∥]Eduard-Zintl-Institut für Anorganische und Physikalische Chemie, Technische Universität Darmstadt, Petersenstrasse 20, D-64287 Darmstadt, Germany

Supporting Information

ABSTRACT: Reaction of iron(II) thiocyanate with an excess of *trans*-1,2-bis(4-pyridyl)-ethylene (bpe) in acetonitrile at room temperature leads to the formation of $[Fe(NCS)_2(bpe)_2\cdot(bpe)]$ (**1**), which is isotypic to its Co(II) analogue. Using slightly different reaction conditions the literature known compound $[Fe(NCS)_2(bpe)_2(H_2O)_2]$ (**2**) was obtained as a phase pure material. Simultaneous differential thermoanalysis and thermogravimetry prove that the hydrate **2** transforms into the anhydrate $[Fe(NCS)_2(bpe)_2]$ (**3**), that decomposes on further heating into the new ligand-deficient 1:1 compound of composition $[Fe(NCS)_2(bpe)]_n$ (**4**), which can also be obtained directly by thermal decomposition of **1**. Further investigations reveal that **4** can also be prepared under solvothermal conditions, and single crystal structure analysis shows that the iron(II) cations are linked via μ-1,3 bridging thiocyanato anions into chains, that are further connected into layers by the bpe ligands. Magnetic measurements, performed on powder samples, prove that **1** and **2** show only Curie–Weiss behavior, whereas in **4** antiferromagnetic ordering with a Néel temperature of 5.0 K is observed. At $T < 4.0$ K a two-step metamagnetic transition occurs at applied magnetic fields of 1300 and 1775 Oe. The magnetic properties are discussed and compared with those of related compounds.

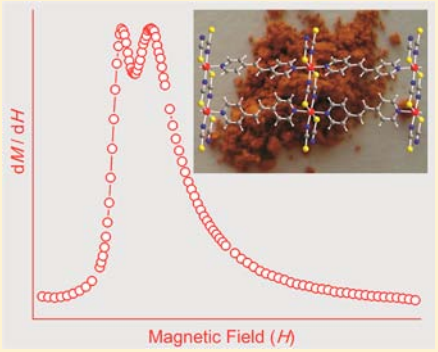

INTRODUCTION

Recently, investigations on the synthesis and the properties of new coordination polymers, metal–organic frameworks (MOFs), and inorganic–organic hybrid compounds are a major field of chemical research.[1] In this context, materials with cooperative magnetic phenomena are of special interest, which includes also metamagnetic behavior or single chain magnets that show slow relaxations of the magnetization below a specific temperature.[2] To mediate magnetic exchange interactions usually paramagnetic transition metal cations are connected by small-sized ligands, and therefore, a large number of such compounds are reported in literature with some of them based on, e.g., transition metal azides.[3] In contrast, similar compounds based on other three atomic anionic ligands like, e.g., thio- or selenocyanates are less reported because the *N*-terminal coordination is frequently preferred. Therefore, we have started systematic investigations on the synthesis of μ-1,3-bridged transition metal thio- and selenocyanato coordination polymers that contain additional neutral *N*-donor coligands in order to investigate the correlations between the structures and the magnetic properties of such compounds in more detail.

However, in some cases, such compounds cannot be prepared in the solution phase, and therefore, we have developed a different approach for their synthesis, which is based on thermal decomposition of precursors with terminal *N*-bonded thiocyanato anions that transform into μ-1,3-bridging coordination polymers upon heating.[4] In the course of these investigations we have reported on 1D coordination polymers of the general composition $[M(NCS)_2(pyridine)_2]_n$ with M = Mn, Fe, Co, and Ni and $[Co(NCSe)_2(pyridine)_2]_n$.[5] Surprisingly, we have found that the compounds based on Co(II) show single chain magnetic behavior, which was never observed before in a thiocyanato coordination polymer. In this context it is noted that the Fe(II) analogue was already investigated by Foner et al., who found that a metamagnetic transition occurs in this compound.[6] Continuing our research we investigated the isotypic selenocyanato compound to explore the influence of stronger intrachain interactions on the magnetic behavior, and we still have found metamagnetic behavior with a

Received: October 30, 2012
Published: December 31, 2012

   dx.doi.org/10.1021/ic302370n | *Inorg. Chem.* 2013, 52, 1061–1068

significant increase of the critical field.[7] Surprisingly, in contrast to its thiocyanato analogue a slow relaxation of the magnetization is observed indicating 1D ferromagnetic behavior. In the course of our systematic work we also investigated layered coordination polymers with *trans*-1,2-bis(4-pyridyl)-ethylene (bpe) as coligand which are structurally related to the pyridine coordination polymers.[8] In these compounds μ-1,3-bridged metal(II) thiocyanato chains are observed, which in contrast to the pyridine compounds are linked into layers by the relatively large bpe ligands. Magnetic measurements of the Co(II) compound reveal that metamagnetic behavior occurs with a slow relaxation of the magnetization above the critical field (H_C) and antiferromagnetic behavior below H_C where the slow relaxation of the magnetization is still present.[8] On the basis of these findings we decided to prepare compounds with iron(II) thiocyanate and bpe as coligand to study its magnetic properties.

In this context especially the μ-1,3-bridging compound would be of interest, because the question arises as to if it will also show metamagnetic behavior, which might be accompanied by a slow relaxation of the magnetization. It is noted that the compound of composition $[Fe(NCS)_2(bpe)_2(H_2O)_2]$ was already reported in literature.[9] Its crystal structure consists of discrete complexes, in which the metal centers are coordinated by two terminal *N*-bonded thiocyanato anions, two water molecules, and two terminal bpe ligands. Interestingly, thermogravimetric investigations indicate that the water can be removed on heating in the first step and that a compound of composition $Fe(NCS)_2(bpe)$ might form in the second step. However, none of these intermediates were isolated and identified, and the thermal behavior was not discussed in detail. Following our research we have found a new compound of composition $[Fe(NCS)_2(bpe)_2{\cdot}(bpe)]$, and we have investigated this compound as well as the hydrate for their thermal behavior. Both compounds can be transformed into the corresponding μ-1,3 bridging compound on heating, but we have also found that single crystals of this compound can directly be prepared from solution. Here we report on these investigations.

SYNTHETIC INVESTIGATIONS

Reaction of $FeSO_4{\cdot}7H_2O$ with an excess of the neutral coligand *trans*-1,2-bis(4-pyridyl)-ethylene (bpe) leads to the pure phase formation of a new ligand-rich 1:3 compound of composition $[Fe(NCS)_2(bpe)_2{\cdot}(bpe)]$ (**1**). XRPD measurements reveal that it is isotypic to its Co(II) analogue, in which the metal centers are coordinated by two terminal-*N*-bonded thiocyanato anions and four bpe ligands within an octahedral geometry (see Figure S1).[8] If less coligand is used in the synthesis the literature known compound $[Fe(NCS)_2(bpe)_2(H_2O)_2]$ (**2**) is obtained as a pure phase (see Figure S2).[9] Simultaneous thermogravimetry and differential thermoanalysis of compound **1** show two endothermic mass steps of which the first one might correspond to the transformation into a ligand-deficient 1:1 compound of composition $[Fe(NCS)_2(bpe)]_n$ (**4**), which decomposes on further heating (see Figure S3 and Table S1). However, in contrast to **1**, for the hydrate **2** three distinct endothermic mass steps are observed of which the first one corresponds to the formation of an anhydrate of composition $Fe(NCS)_2(bpe)_2$ (**3**), which loses half of the bpe ligands on further heating transforming into a compound of the same composition as observed for the intermediate obtained by thermal composition of **1** (see Figure S3 and Table S1). To verify the nature of the intermediates additional TG experiments were performed and stopped after each mass step and the residues were investigated by IR-spectroscopy, CHNS analysis, and X-ray powder diffraction. Elemental analysis confirms the supposed composition calculated from the experimental mass loss, and IR spectroscopy reveals that in **1** and **2** only terminal *N*-bonded thiocyanato anions are present, whereas in **4** the asymmetric stretching vibration $\nu_{as}(CN)$ is shifted to 2096 cm^{-1} indicating the presence of μ-1,3-bridging thiocyanato anions (see Figure S4−S6 and Table S2). For the anhydrate **3** two bands are found at 2052 and 2101 cm^{-1}, and XRPD measurements reveal that the sample is of very poor crystallinity and that at least to different crystalline phases are present (see Figure S7−S8). Therefore, no further investigations were performed on this compound. However, XRPD measurements show that compound **4** is isotypic to its Co analogue and that the same crystalline phase is obtained independent of whether **1** or **2** is thermally decomposed (see Figure S9). Finally, compound **4** was additionally investigated by Mössbauer spectroscopy, which shows only one doublet with an isomer shift of δ_{IS} = 1.1 mm/s and a quadrupole splitting of ΔE_Q = 3.5 mm/s, which is in good agreement with that expected for a iron(II) cation (see Figure S10).[10] On the basis of this information we tried to prepare **4** also in the solution phase at room-temperature, and under solvothermal conditions we obtained single crystals that were suitable for structure determination (see Figure S11−S12).

Crystal Structure of $[Fe(NCS)_2(bpe)]_n$ (4). Compound **4** crystallizes in the centrosymmetric space group $P\bar{1}$ with two formula units in the unit cell (Table 3). The asymmetric unit consists of two crystallographically independent iron(II) cations and two bpe ligands that are located on centers of inversion as well as two independent thiocyanato anions that occupy a general positions (Figure 1). Each iron(II) cation is coordinated by two *trans*-oriented *N*-bonded and two *S*-bonded thiocyanato anions as well as two *trans*-oriented *N*-bonded bpe ligands in a slightly distorted octahedral geometry (Figure 1 and Table 1). The Fe−N distances to the neutral bpe ligand are significantly shorter than those to the negatively charged thiocyanato N anions and are in the range of those in similar compounds. The Fe−S distances correspond exactly to those values reported in literature for similar compounds.[5b,11] Both bpe ligands are *trans*-configurated and are exactly coplanar. However, there are no significant differences in the coordination geometry of both crystallographically independent metal cations (Table 1).

In the crystal structure the metal cations are connected via two μ-1,3-bridging thiocyanato anions into chains, in which the two crystallographically independent metal cations alternate with an Fe···Fe distance of 5.702 Å (Figure 2, top).

These chains are further linked into layers by the bpe ligands. Formally, there are two crystallographically independent −Fe−bpe−Fe− chains constructed by either Fe1 or Fe2, and the Fe···Fe distance within these chains amounts to 13.783 Å. It is noted that the bpe ligands in the two independent −Fe−bpe−Fe− chains are oriented exactly perpendicular to each other (Figure 2, top and bottom).

MAGNETIC PROPERTIES

The compounds **1** and **2** with metal cations not linked by the thiocyanato anions are not expected to show cooperative magnetic phenomena. Consequently, our magnetic measurements on both compounds show only paramagnetic behavior,

dx.doi.org/10.1021/ic302370n | Inorg. Chem. 2013, 52, 1061−1068

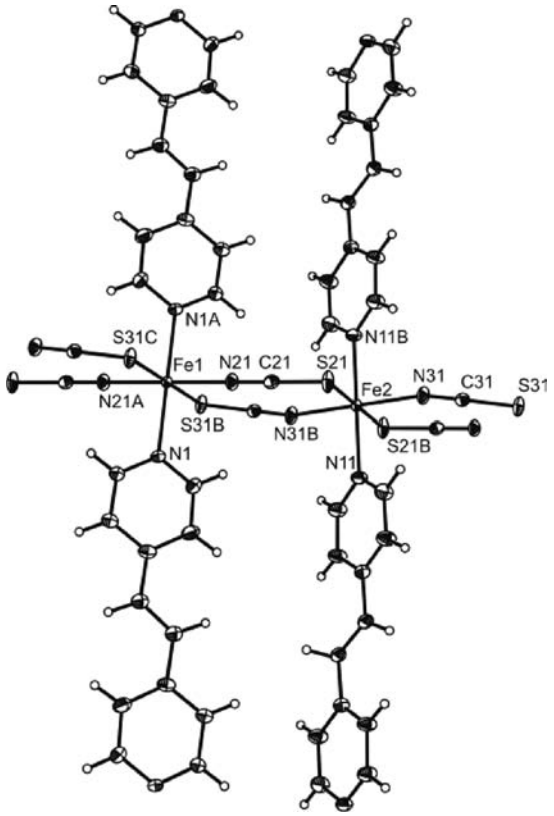

Figure 1. Crystal structure of **4** with view of the coordination sphere of the iron(II) cations with labeling and displacement ellipsoids drawn at the 50% probability level. Symmetry codes: A = $-x$, $-y + 1$, $-z$; B = $-x + 1$, $-y + 2$, $-z + 1$; C = $x - 1$, $y - 1$, $z - 1$.

Table 1. Selected Bond Lengths/Å and Angles/deg for Compound 4

Fe(1)–N(1)	2.201(3)	Fe(2)–N(11)	2.192(3)
Fe(1)–N(21)	2.098(3)	Fe(2)–N(31)	2.108(3)
Fe(1)–S(31B)	2.5995(9)	Fe(2)–S(21)	2.5973(10)
N(21A)–Fe(1)–N(21)	180.0	N(31)–Fe(2)–N(31B)	180.0
N(21A)–Fe(1)-N(1A)	90.08(11)	N(31)–Fe(2)–N(11)	89.64(12)
N(21)–Fe(1)–N(1A)	89.92(11)	N(31B)–Fe(2)–N(11)	90.36(12)
N(21A)–Fe(1)-S(31B)	87.92(9)	N(31)–Fe(2)–S(21)	86.26(9)
N(21)–Fe(1)–S(31B)	92.08(9)	N(31B)–Fe(2)–S(21)	93.74(9)
N(1A)–Fe(1)–S(31B)	90.03(8)	N(11B)–Fe(2)-S(21B)	89.47(9)
N(1)–Fe(1)–S(31B)	89.97(8)	N(11)–Fe(2)–S(21B)	90.53(9)

and the fit of the magnetic data according to the Curie–Weiss law [$\chi_M = C/(T - \theta)$] reveals a Weiss constant, which is practically zero, and effective magnetic moments μ_{eff} of 5.62 μ_B (g = 2.30) for **1** and of 5.23 μ_B (g = 2.14) for **2**, which are slightly higher than the spin-only value of 4.89 expected for the high-spin Fe^{2+} (S = 2, g = 2) (see Figure S13 and Table S3). In contrast, compound **4**, composed of magnetic chains connected through bpe coligands into planes not coupled themselves by chemical bonds, is expected to show rich magnetic behavior. Because the coordination octahedron of Fe in this compound has one distinctive (most elongated) direction along Fe–S

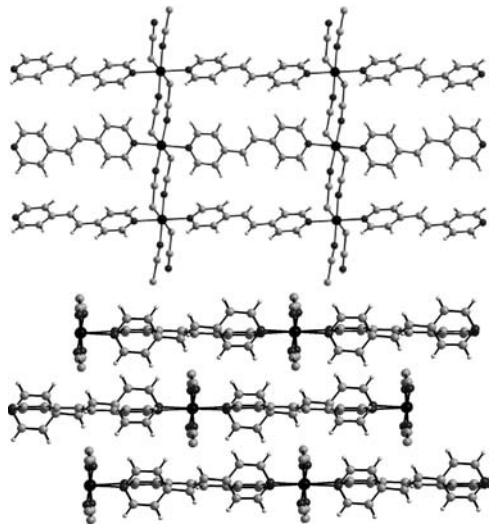

Figure 2. Crystal structure of **4** with view onto (top) and in the direction of (bottom) the layers.

bond, the magnetic easy axis is expected to lie in this direction; i.e., it is declined 58° to Fe1–Fe2–Fe1 chain direction. Below, magnetic measurements data for **4** are presented. Figure 3

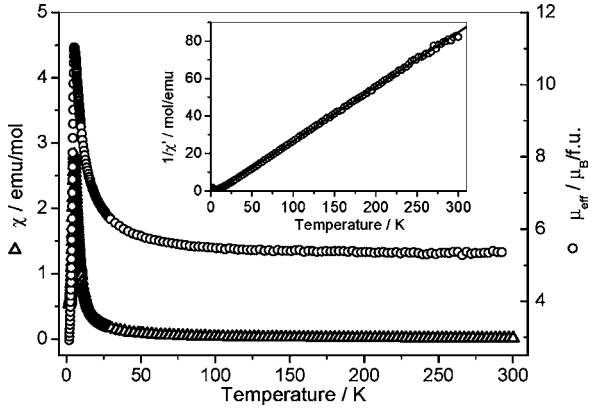

Figure 3. Molar susceptibility and effective magnetic moment for **4** measured in dc field of 200 Oe plotted as a function of temperature. In the inset the reciprocal susceptibility vs temperature is shown; the straight line is a linear fit.

presents data obtained in a magnetic field of 200 Oe. In the main graph the temperature dependence of magnetic susceptibility and of the effective magnetic moment (μ_{eff} = $[8\chi_{mol}\cdot T]^{1/2}$) are shown. In the inset the reciprocal magnetic susceptibility is shown as function of temperature.

A bunch of similar zero field cooling curves, measured in a limited temperature range 2–15 K but drawn in magnetization units, are shown in Figure S14. It is seen that with increasing magnetic field the maximum of susceptibility moves to lower temperatures and diffuses. The observed susceptibility maximum is typical for the phase transition from the paramagnetic to the antiferromagnetic state. In a low field of 200 Oe it occurs at the Néel temperature of 5.3 K but moves to 5.0 K in 1000 Oe. As seen in Figure 3, the effective magnetic moment increases during cooling from room temperature. This fact, together with the positive Curie–Weiss temperature, equal to +8.0 K, proves dominant ferromagnetic intrachain interaction J_{intra}. By assuming the high spin of Fe(II) ion S = 2, g-factor

dx.doi.org/10.1021/ic302370n | Inorg. Chem. 2013, 52, 1061–1068

equal to 2.2 may be obtained from the Curie–Weiss law. The exchange constant J_{intra} = 2 K can be estimated by using the mean field relation $\theta = zJS(S+1)/3k_B$ with z equal 2 (z is a number of nearest neighbors). In the case of the Ising or anisotropic Heisenberg linear system a more exact J_{intra} value may be obtained from the slope of $\ln(\chi T)$ versus T^{-1} dependence, with $\chi(T)$ registered in a small magnetic field (100 Oe; see Figure 4). With our Hamiltonian

$$\mathcal{H} - -J_{intra}\sum_i S_i \cdot S_{i+1} + D\sum_i S_{i,z}^2 + \mu_B H \cdot g \cdot \sum_i S_i$$

the expression for slope is $2J_{intra}S^2$. The value of J_{intra} thus obtained is equal to1.3 K.

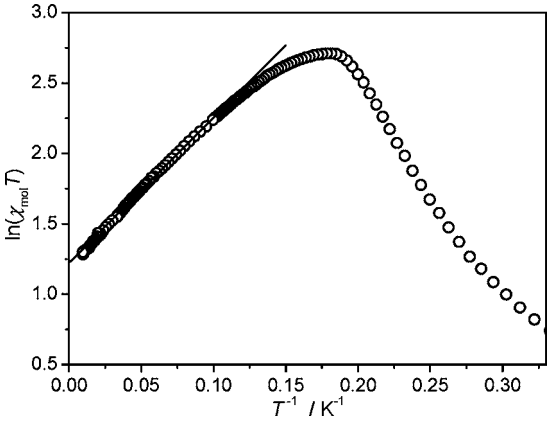

Figure 4. Reciprocal temperature dependence of $\ln(\chi_{mol} \cdot T)$ for **4**. Solid line is a linear fit.

Another important magnetic parameter is the single ion anisotropy. It can be estimated from magnetization (M) versus field (H) measurements. In Figure 5 $M(H)$ dependence measured at the temperature of 1.5 K is shown. It was registered with a small field step, so that an interesting behavior was not overlooked. Namely, by increasing magnetic field from zero, initially the slope of magnetization curve is small, typical for an antiferromagnet, in accordance with our susceptibility measurements. By further increasing the field at some its critical value H_C ≈1.0 kOe, a sharp upraise of magnetization was observed. The magnetization curves shown in the Figure 5 were measured in both field directions (along a loop). A small hysteresis is seen only in the vicinity of H_C (Figure 5, bottom panel).

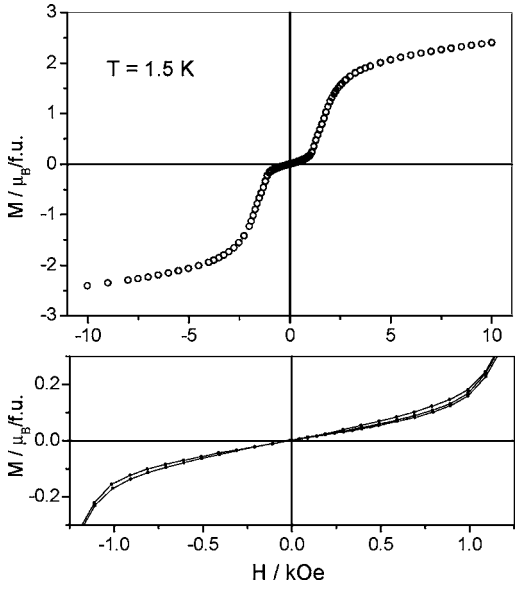

Figure 5. Magnetization vs magnetic field measured at 1.5 K for **4**. Bottom panel is the central part of the upper panel in enlargement showing small hysteresis in the region of 1 kOe.

In Figure 6b magnetization curves are plotted in the full accessible field range, i.e., up to 70 kOe. In Figure 6a they are presented as a function of H/T. For comparison, the Brillouin curve for S = 2 is also shown in Figure 6. At lower magnetic fields the $M(H)$ curves go above the Brillouin curve, which indicates dominant ferromagnetic character in this compound. At higher fields, especially at lowest temperatures, the $M(H)$ curves go lower. This demonstrates the significant role of anisotropy. The single ion anisotropy parameter D can be estimated from of $M(H)$ curve extrapolated to intersection with the ordinate corresponding to the expected saturation value $M(H_a) = g\mu_B S$, see Figure 6b.[12] This procedure is right for the case of the uniaxial anisotropy. From the relation

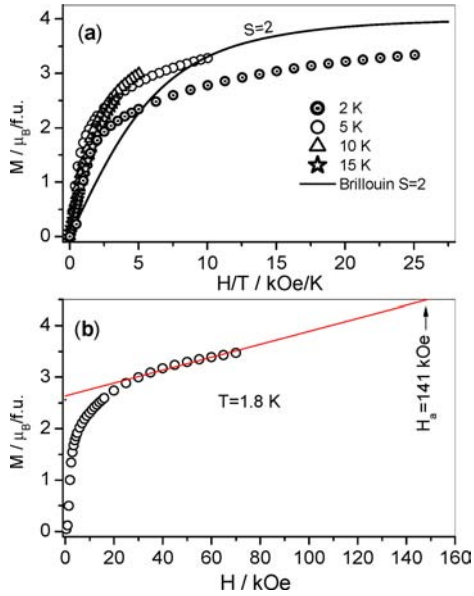

Figure 6. Field dependent magnetization data for **4**. (a) M as a function of H/T; comparison with the Brillouin function for S = 2 is also shown. (b) M as a function of H. The solid line is an extrapolation to the intersection with the predicted saturation value of M.

$$DS^2 = \frac{1}{2} g\mu_B S H_a$$

substituting g = 2.2 and H_a = 141 kOe and assuming the high spin S = 2 for Fe^{2+} ion, the value of $|D|$ equal to 5.2 K is obtained. This is a large value, considerably greater than the intrachain exchange interaction (~1.5 K). This fact points out that by the field transition at H_C we are dealing with a metamagnetic (spin-flip) transition by which the antiferromagnetic state is broken by the field.[13] This should be not mixed with the so-called spin-flop transition occurring by a low anisotropy, when antiferromagnetic direction jumps to the direction, which is perpendicular to field.[13]

In the next step the ac dynamic properties are presented. Figure 7 shows the temperature dependence of two alternate

dx.doi.org/10.1021/ic302370n | Inorg. Chem. 2013, 52, 1061–1068

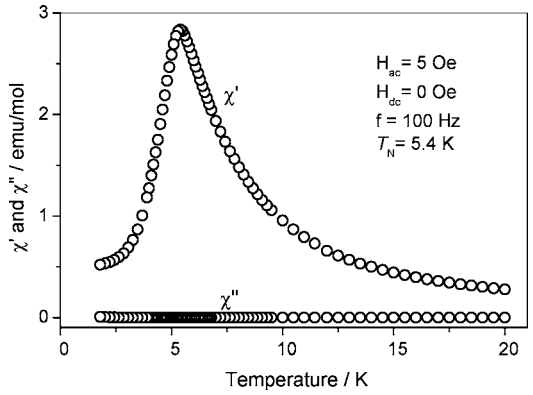

Figure 7. Temperature dependence of ac susceptibility for **4** measured at the frequency of 100 Hz and zero dc magnetic field.

current (ac) susceptibility components χ' and χ'' measured in zero dc field at frequency 100 Hz. The maximum of χ' falls at 5.5 K, so at a little greater temperature than the maximum of dc susceptibility, observed at 5.0 K in the field of 1000 Oe; however, this is expected for an antiferromagnet. As seen in Figure 7, there is no χ'' response near the maximum of χ', which, together with no frequency dispersion of χ' (see Figure S15), proves that the observed susceptibility maximum is a manifestation of phase transition to the antiferromagnetic state.

Alternating current susceptibility was also measured as a function of dc field. These data, obtained at T = 2.1 K, are shown in Figure 8 (see also Figure S16 for a higher field range).

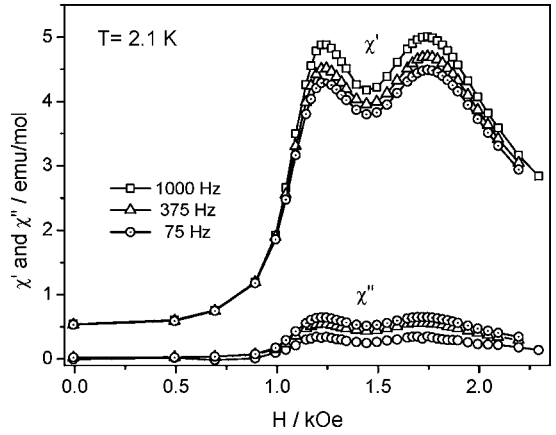

Figure 8. Alternating current susceptibility vs external field dependence for **4** measured at T = 2.1 K for three various frequencies. Solid lines are guides for the eye.

Two humps are seen at H_{C1} = 1300 and H_{C2} = 1775 Oe for χ' as well as for χ''. By frequency change no difference in response of χ' and χ'' for both humps was observed (see also Figure S17). The relaxation observed at humps is far from the Debye relaxation (see Figure S18). The same picture as for χ' may be obtained by differentiating the magnetization curve (see Figure S19). Many such ac curves, as in Figure 8, were registered for various temperature points. With increasing temperature two humps approach one another and coalesce into one. The humps were fitted with two asymmetric Gaussian, and their found positions were used to construct the phase diagram, which is shown in Figure 9. The presence of two χ'' maxima and their frequency dispersion prove that an intermediary ferrimagnetic phase (IFiM) appears with field increasing before

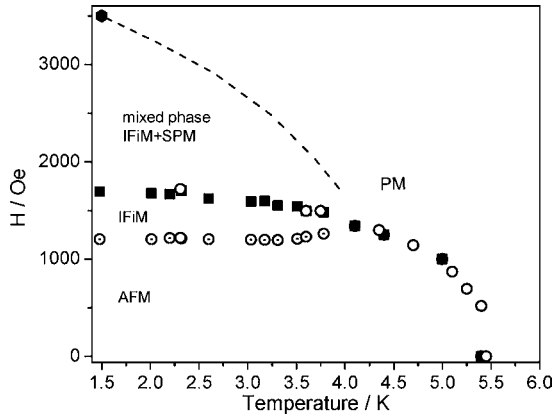

Figure 9. Phase diagram for **4**. The various experimental points were collected during several experimental sessions. The dash−dot line is an intentionally drawn phase boundary: AFM, antiferromagnetic phase; IFiM, intermediate ferrimagnetic phase; SPM, saturated paramagnetic phase; PM, paramagnetic phase.

the saturated paramagnetic phase (SPM) appears. Due to demagnetization effect both transitions are not complete.[14] The mixed phase region above H_{C2} is partially ferrimagnetic and partially paramagnetic, but with increasing magnetic field the mixed phase gradually transforms to the saturated paramagnetic phase. This occurs at the new phase boundary at H_{C3} for which the lowest temperature point was estimated as the field where χ'' disappears (the H_{C3} boundary is intentionally drawn with a dash−dot line).[15] It should be noted that we are dealing with a powder sample, where grains have various orientation with respect to the field direction; thus, the observed transitions are diffused.

Discussion of the Magnetic Properties. The one-dimensional ferromagnetic chains with easy axis anisotropy are expected to show slow magnetic relaxations; however, they were not observed for $[Fe(NCS)_2(bpe)]_n$ studied in this work. In zero magnetic field this compound is antiferromagnetic with Néel temperature of 5.0 K. Certainly, there exist remarkable antiferromagnetic interchain interactions. In the critical field $H_C \approx$ 1.3 kOe the metamagnetic transition occurs when the antiferromagnetic interaction is overcome by field. For analysis of the magnetic behavior it is good to point out the possible paths for magnetic interactions. We have ferromagnetic chains $[Fe(\mu\text{-}NCS)_2Fe]_n$, linked into layers through bpe coligands. There is no chemical bond between the layers. The magnetic interlayer coupling is possible only through space (dipolar) interactions. It should be noted that because of rather short interlayer Fe−Fe distances (the shortest is 8.886 Å) the interchain-interlayer Fe−Fe interactions may be comparable with interchain−intralayer Fe−Fe interaction. There were reports that the exchange interactions, transferred on such long distances as ∼12 Å, may be not negligible.[16] On the other hand, it is known that in ferromagnetic chains the superspins develop, which act cooperatively on every distance, may give a relatively large critical temperature of transition to the ordered state.[17] When magnetic field is applied, the weakest antiferromagnetic coupling is broken. The effective value of this interaction can be estimated from the following relation (for T = 0 K), derived by equating the change of the exchange energy and Zeeman energy by the low field transition

$$zJ'S^2 = g\mu_B SH_c$$

dx.doi.org/10.1021/ic302370n | Inorg. Chem. 2013, 52, 1061−1068

where zJ' is the effective weakest interchain interaction. The value of zJ' equal to ~ -0.08 cm^{-1} (0.11 K) is obtained. Thus, we obtain the ratio zJ'/J_{intra} equal to $0.11/1.3 \cong 0.08$. This is a rather large value, which can make slow relaxations impossible.

In this context it is worth comparing magnetic properties of **4** and other relative compounds studied by our group and other researchers. The isotypic compound $[Co(NCS)_2(bpe)]_n$ is an antiferromagnet with the Néel temperature T_N = 4.3 K.[8] With increasing field it shows a metamagnetic transition (H_C = 0.65 kOe), but there is no sign of an intermediary phase (one step transition).[8] Below T_N, in field near H_C the compound shows slow relaxations typical for single chain magnets. Slow relaxation of the magnetization with a narrow relaxation time distribution is also observed in the chain compound $[Co(NCS)_2(pyridine)_2]_n$, where the magnetic chains are not coupled through coligands into layers.[5a] Interestingly, here, no metamagnetic transition in contrast to the layer compound $[Co(NCS)_2(bpe)]_n$ is observed, indicating that the bidentate coligand bpe might be involved in the magnetic exchange.[5a,8] However, it should be noted that $[Fe(NCS)_2(pyridine)_2]_n$, which is isotypic to $[Co(NCS)_2(pyridine)_2]_n$, shows metamagnetic transition ($H_C \sim 0.7$ kOe) at 4.2 K which means that coupling of the ferromagnetic chains through bpe into layers might not be crucial for a metamagnetic transition.[6]

$[Fe(NCS)_2(pyridine)_2]_n$ compound, similarly as its bpe analogue, does not show slow relaxations of the magnetization.[5b] Interestingly, if the anionic ligand in $[Fe(NCS)_2(pyridine)_2]_n$ is exchanged by selenocyanato the metamagnetic behavior is still present but a slow relaxation of the magnetization is observed above H_C.[7] The SCM behavior might be related to an increase in the intrachain interaction in the selenocyanato compound, retrieved from the slope of the $\ln(\chi T)$ versus T^{-1} curves (Table 2). For the Fe compound **4** this value was estimated to be 1.3 K (Table 2). However, for a slow relaxation of the magnetization a large energy barrier for spin reversal is needed. It depends on both the intrachain interaction J_{intra} and the single ion anisotropy D. Therefore, we have estimated the D values for the three Fe compounds from the magnetization curves. It appears that the anisotropy for the pyridine coligand is higher than for bpe coligand. This fact, together with lower value of J_{intra} for **4** and by assumption that weakest interchain interaction is comparable in all three compounds, explains why no slow relaxation of the magnetization was observed in **4** (Table 2). The reason why SCM behavior is found in the corresponding Co compounds might be predominantly related to the higher anisotropy of Co(II) compared to Fe(II).[5a]

Table 2. Comparison of Magnetic Properties for Three Related Compounds: $[Fe(NCS)_2(bpe)]_n$ (4), $[Fe(NCS)_2(pyridine)_2]_n$ (A), and $Fe(NCSe)_2(pyridine)_2]_n$ (B)[5b,7]

	4	A	B
J_{intra} (K)	1.3	1.32	2.0
D (K)	4	8	6.6
H_C (Oe)	1300; 1775	1200	1300
slow relaxations	not observed	not observed	observed

An interesting question is why in the family of compounds discussed above the metamagnetic transition appears and sometimes it is two-step, sometimes one-step transition. The following linear chain compounds show two-step transition: $CoCl_2{\cdot}2H_2O$, $CoBr_2{\cdot}2H_2O$, $FeCl_2{\cdot}2H_2O$, $CoCl_2(pyridine)_2$.[18] It was shown that the change of magnetic moment at the first transition is exactly $^1/_2$ of the change at the second transition.[18c,d,19] Narath explained the two-step transition by six-sublattices model, which needed four exchange integrals.[18d,c,19,18b] There is some difficulty in applying this model to our case because only two exchange paths through chemical bonds may be pointed out. Thus, dipolar interaction should also contribute to the appearance of metamagnetic transitions.

CONCLUDING REMARKS

In the present contribution we have reported on the synthesis of a new Fe thiocyanato coordination polymer that was synthesized in the beginning by thermal decomposition but later could be also prepared in the solution phase. This compound is composed of ferromagnetic iron thiocyanato chains that are linked into layers by neutral bpe coligands. At low field this compound shows antiferromagnetic ordering, but on increasing field an unusual two-step metamagnetic transition is observed. It is noted that the isotypic compound $[Co(NCS)_2(bpe)]_n$ also shows metamagnetic behavior, but because of the higher anisotropy of Co(II) slow relaxation of the magnetization is additionally observed. The origin of metamagnetic transition is still unclear. On the one hand, the fact that $[Fe(NCS)_2(bpe)]_n$ (**4**) and $[Co(NCS)_2(bpe)]_n$ show metamagnetic behavior but $[Co(NCS)_2(pyridine)_2]_n$ does not show, indicates that the coligand bpe is involved in the magnetic exchange interactions. On the other hand, $[Fe(NCS)_2(pyridine)_2]_n$ shows metamagnetic transition, which means that for metamagnetic transition the intermediary of bpe is not needed. To investigate this question in more detail the compounds with identical coordination topology must be prepared, in which the ferromagnetic chains are connected by coligands that cannot mediate magnetic exchange interactions. Therefore, this will be the subject of further investigations.

Relatively large interchain magnetic interactions in $[Fe(NCS)_2(bpe)]_n$ may be responsible for the absence of slow magnetic relaxation in this compound.

EXPERIMENTAL SECTION

Synthesis. $FeSO_4{\cdot}7H_2O$ and KNCS were obtained from Alfa Aesar, and *trans*-1,2-bis(4-pyridyl)-ethylene was obtained from Sigma Aldrich. All chemicals were used without further purification. All crystalline powder were prepared by stirring the reactants in solution for 3 days at room temperature. The residues were filtered off, washed with water and diethyl ether, and dried in air. The identity and purity of all compounds were checked by XRPD (see Figures S1–S2), EDAX measurements (see Table S4), IR spectroscopy (see Figures S4–S7 and Table S2), and CHNS analysis.

Synthesis of $[Fe(NCS)_2(bpe)_2{\cdot}(bpe)]$ (1). A dark red polycrystalline powder of compound **1** was obtained by the reaction of $FeSO_4{\cdot}7H_2O$ (47.1 mg, 0.15 mmol), KNCS (29.3 mg, 0.3 mmol), and *trans*-1,2-bis(4-pyridyl)-ethylene (104.6 mg, 0.6 mmol) in 1 mL of acetonitrile (see Figure S20). Yield based on $FeSO_4{\cdot}7H_2O$: 105.9 mg (98.3%). Calcd for $C_{38}H_{30}FeN_8S_2$ (718.68): C 63.51, H 4.21, N 15.59, S 8.92. Found: C 63.25, H 4.14, N 15.33, S 8.97. IR (KBr): ν_{max} = 2051 (s), 1601 (m), 1411 (m), 1413 (m), 1213 (m), 1009 (m), 962 (m), 830 (m), 813 (m), 548 (s), 482 (w) cm^{-1} (see Figure S4 and Table S2).

Synthesis of $[Fe(NCS)_2(bpe)_2(H_2O)_2]$ (2). A red crystalline powder of compound **2** was prepared by reaction of $FeSO_4{\cdot}7H_2O$ (69.5 mg, 0.25 mmol), KNCS (48.5 mg, 0.5 mmol), and *trans*-1,2-bis(4-pyridyl)-ethylene (92.0 mg, 0.5 mmol) in 3 mL of water (see Figure S20). Yield based on $FeSO_4{\cdot}7H_2O$: 139.6 mg (97.6%). Calcd for $C_{26}H_{24}FeN_6O_2S_2$ (572.49): C 54.55, H 4.23, N 14.68, S 11.20.

dx.doi.org/10.1021/ic302370n | Inorg. Chem. 2013, 52, 1061–1068

Found: C 54.31, H 4.19, N 14.56, S 11.33. IR (KBr): ν_{max} = 3414 (w), 2085 (s), 1608 (s), 1424 (m), 1013 (m), 971 (m), 826 (m), 548 (m) cm^{-1} (see Figure S5 and Table S2).

Synthesis of $[Fe(NCS)_2(bpe)_2]$ (3). This compound can only be obtained as residue in the first TG step of the thermal decomposition reaction of compound $[Fe(NCS)_2(bpe)_2(H_2O)_2]$ (**2**). Calcd for $C_{26}H_{20}FeN_6S_2$ (536.46): C 58.21, H 3.76, N 15.67, S 11.95. Found: C 58.24, H 3.64, N 15.41, S 12.52. IR (KBr): ν_{max} = 3434 (w), 2100 (s), 2052 (s), 1605 (s), 1503 (w), 1424 (m), 1112 (m), 1015 (m), 829 (m), 619 (m), 553 (m) cm^{-1} (see Figure S7 and Table S2).

Synthesis of $[Fe(NCS)_2(bpe)]_n$ (4). Single crystals suitable for X-ray structure determination were obtained by the reaction of $FeSO_4 \cdot 7H_2O$ (166.8 mg, 0.6 mmol), KNCS (116.5 mg, 1.2 mmol), and *trans*-1,2-bis(4-pyridyl)-ethylene (27.6 mg, 0.15 mmol) in 1 mL of water in a closed test tube at 120 °C for three days (see Figure S12). On cooling, red single crystals were obtained. Large amounts of a light red polycrystalline powder can be obtained by reaction of $FeSO_4 \cdot 7H_2O$ (166.8 mg, 0.6 mmol), KNCS (116.5 mg, 1.2 mmol), and *trans*-1,2-bis(4-pyridyl)-ethylene (110.4 mg, 0.6 mmol) in 4 mL of water (see Figure S20). Yield based on $FeSO_4 \cdot 7H_2O$: 208.7 mg (98.2%). Calcd for $C_{14}H_{10}FeN_4S_2$ (354.23): C 47.47, H 2.85, N 15.82, S 18.10. Found: C 47.32, H 2.75, N 15.63, S 19.72. IR (KBr): ν_{max} = 2095 (s), 1606 (s), 1426 (m), 1015 (m), 969 (m), 826 (s), 551 (s), 466 (m) cm^{-1} (see Figure S6 and Table S2).

Spectroscopy. IR data were measured using an ATI Mattson Genesis Series FTIR Spectrometer, control software: WINFIRST, from ATI Mattson.

Elemental Analysis. CHNS analyses were performed using an EURO EA elemental analyzer, fabricated by EURO VECTOR Instruments and Software.

Differential Thermal Analysis and Thermogravimetry. DTA-TG measurements were performed in nitrogen atmosphere (purity: 5.0) in Al_2O_3 crucibles using a STA-409CD thermobalance from Netzsch. The instrument was calibrated using standard reference materials. All measurements were performed with a heating rate of 4 K min^{-1} and a flow rate of 75 mL min^{-1}.

X-ray Powder Diffraction (XRPD). XRPD measurements were performed using a PANalytical X'Pert Pro MPD reflection powder diffraction system with Cu Kα radiation (λ = 154.0598 pm) equipped with a PIXcel semiconductor detector from PANanlytical.

Energy Dispersive X-ray Analysis. EDAX measurements were performed using a Philips XL30 ESEM which is equipped with an EDAX device.

Mössbauer Spectroscopy. Mössbauer spectrum was recorded on a self-constructed spectrometer using linear transmission geometry. As the source rhodium-embedded ^{57}cobalt with an activity of 25 mCurie is used, and all Mössbauer parameters were calculated with respect to a 25 μm thick foil of iron.

Magnetic Measurements. Magnetic measurements were performed using a PPMS (physical property measurement system) from Quantum Design, which was equipped with a 9 T magnet, and using a MPMS-2 SQUID (superconducting quantum interference devices) from Quantum Design, which is equipped with a 7 T magnet. Some measurements were also performed with a LakeShore ac susceptometer/dc magnetometer, model 7225. Diamagnetic corrections were applied with the use of the tabulated Pascal's constants.

Single-Crystal Structure Analysis. All investigations were performed with an imaging plate diffraction system (IPDS-2) with Mo Kα radiation from STOE & CIE. The structure solution was done with direct methods using SHELXS-97, and structure refinements were performed against $|F|^2$ using SHELXL-97.[20] A numerical absorption correction was applied using X-Red (Version 1.31) and X-Shape (Version 2.11) of the Program Package X-Area.[21] All hydrogen atoms were positioned with idealized geometry and were refined with fixed isotropic displacement parameters $[U_{iso}(H) = -1.2 \cdot U_{eq}(C)]$ using a riding model with d_{C-H} = 0.95 Å. All non-hydrogen atoms were refined with anisotropic refinement parameters. Details of the structure determination are given in Table 3.

CCDC-907748 (**4**) contains the supplementary crystallographic data for this paper. These data can be obtained free of charge from the Cambridge Crystallographic Data Centre via http://www.ccdc.cam.ac.uk/.

Table 3. Selected Crystal Data and Results of the Structure Refinement for $[Fe(NCS)_2(bpe)]_n$ (4)

	4
formula	$C_{14}H_{10}FeN_4S_2$
ratio M:L	1:1
MW/g mol^{-1}	354.23
cryst syst	triclinic
space group	$P\bar{1}$
a/Å	9.3012(8)
b/Å	9.4487(10)
c/Å	10.3283(9)
α/deg	113.787(11)
β/deg	108.046(10)
γ/deg	94.625(12)
V/Å^3	767.37(12)
T/K	170(2)
Z	2
$D_{calc.}$/g·cm^{-3}	1.533
μ/mm^{-1}	1.251
min/max transm	0.7269/0.8760
θ_{max}/deg	28.06
measured reflns	5747
unique reflns	3509
reflns $[F_o \geq 4\sigma(F_o)]$	2458
params	194
R_{int}	0.0316
R1[a] $[F_o \geq 4\sigma(F_o)]$	0.0486
wR2[b] [all data]	0.01627
GOF	1.065
$\Delta\rho_{max}$, $\Delta\rho_{max}$/e·Å^3	1.320/−0.672

[a] $R1 = \sum||F_o| - |F_c||/\sum|F_o|$. [b] $wR2 = [\sum[w(F_o^2 - F_c^2)^2]/\sum[w(F_o^2)^2]]^{1/2}$.

■ ASSOCIATED CONTENT

Ⓢ Supporting Information

EDAX measurements; experimental XRPD measurements of compound **1**, **2**, **3**, and **4**; IR spectra of compound **1**, **2**, **3**, and **4**, as well as their interpretation; DTA/TG/DTG measurements of compound **1** and **2** and their interpretation; Mössbauer spectrum of compound **4**; and magnetic measurements of compound **1**, **2** and **4**. This material is available free of charge via the Internet at http://pubs.acs.org.

■ AUTHOR INFORMATION

Corresponding Author

*E-mail: cnaether@ac.uni-kiel.de. Fax: +49-431-8801520.

Notes

The authors declare no competing financial interest.

■ ACKNOWLEDGMENTS

We acknowledge financial support by the State of Schleswig-Holstein and the DFG (Project NA 720/3-1). We thank Professor Dr. Wolfgang Bensch for the opportunity to use his experimental facility. Z.T. acknowledges the grant of Ministry of Science and Higher Education, Poland, N N202103238. M.W. acknowledges the Postdoc Programme of the German Academic Exchange Service (DAAD) for financial support.

REFERENCES

(1) (a) Motokawa, N.; Matsunaga, S.; Takaishi, S.; Miyasaka, H.; Yamashita, M.; Dunbar, K. R. *J. Am. Chem. Soc.* **2010**, *132* (34), 11943−11951. (b) Navarro, J. A. R.; Barea, E.; Rodriguez-Dieguez, A.; Salas, J. M.; Ania, C. O.; Parra, J. B.; Masciocchi, N.; Galli, S.; Sironi, A. *J. Am. Chem. Soc.* **2008**, *130* (12), 3978−3984. (c) Braga, D.; Maini, L.; Polito, M.; Scaccianoce, L.; Cojazzi, G.; Grepioni, F. *Coord. Chem. Rev.* **2001**, *216*, 225−248. (d) Wang, X.-Y.; Wang, Z.-M.; Gao, S. *Chem. Commun.* **2007**, 1127−1129. (e) Janiak, C. *Dalton Trans.* **2003**, *14*, 2781−2804. (f) Miller, J. S. *Adv. Mater.* **2002**, *14* (16), 1105−1110. (g) Miller, J. S.; Epstein, A. J. *Angew. Chem., Int. Ed. Engl.* **1994**, *33* (4), 385−415. (h) Vallejo, J.; Castro, I.; Canadillas-Delgado, L.; Ruiz-Perez, C.; Ferrando-Soria, J.; Ruiz-Garcia, R.; Cano, J.; Lloret, F.; Julve, M. *Dalton Trans.* **2010**, *39* (9), 2350−2358. (i) Carranza, J.; Sletten, J.; Lloret, F.; Julve, M. *Inorg. Chim. Acta* **2011**, *371* (1), 13−19. (j) Yuste, C.; Ferrando-Soria, J.; Cangussu, D.; Fabelo, O.; Ruiz-Pérez, C.; Marino, N.; De Munno, G.; Stiriba, S.-E.; Ruiz-García, R.; Cano, J.; Lloret, F.; Julve, M. *Inorg. Chim. Acta* **2010**, *363* (9), 1984−1994. (k) Landee, C. P.; Turnbull, M. M. *Mol. Cryst. Liq. Cryst.* **1999**, *335*, 193−200. (l) Hammar, P. R.; Stone, M. B.; Reich, D. H.; Broholm, C.; Gibson, P. J.; Turnbull, M. M.; Landee, C. P.; Oshikawa, M. *Phys. Rev. B* **1999**, *59*, 1008−1015.

(2) (a) Zhang, X.-H.; Hao, Z.-M.; Zhang, X.-M. *Chem.—Eur. J.* **2011**, *17* (20), 5588−5594. (b) Marvilliers, A.; Parsons, S.; Rivière, E.; Audière, J.-P.; Kurmoo, M.; Mallah, T. *Eur. J. Inorg. Chem.* **2001**, *2001* (5), 1287−1293. (c) Pereira, C. L. M.; Pedroso, E. F.; Stumpf, H. O.; Novak, M. A.; Ricard, L.; Ruiz-García, R.; Rivière, E.; Journaux, Y. *Angew. Chem.* **2004**, *116* (8), 974−976. (d) Tyree, W. S.; Slebodnick, C.; Spencer, M. C.; Wang, G.; Merola, J. S.; Yee, G. T. *Polyhedron* **2005**, *24* (16−17), 2133−2140. (e) Bogani, L.; Sangregorio, C.; Sessoli, R.; Gatteschi, D. *Angew. Chem., Int. Ed.* **2005**, *44* (36), 5817−5821. (f) Bogani, L.; Vindigni, A.; Sessoli, R.; Gatteschi, D. *J. Mater. Chem.* **2008**, *18* (40), 4750−4758. (g) Caneschi, A.; Gatteschi, D.; Lalioti, N.; Sangregorio, C.; Sessoli, R.; Venturi, G.; Vindigni, A.; Rettori, A.; Pini, M. G.; Novak, M. A. *Angew. Chem., Int. Ed.* **2001**, *40* (9), 1760−1763. (h) Miyasaka, H.; Clérac, R. *Bull. Chem. Soc. Jpn.* **2005**, *78* (10), 1725−1748. (i) Sun, H. L.; Wang, Z. M.; Gao, S. *Coord. Chem. Rev.* **2010**, *254* (9−10), 1081−1100. (j) Bałanda, M.; Rams, M.; Nayak, S. K.; Tomkowicz, Z.; Haase, W.; Tomala, K.; Yakhmi, J. V. *Phys. Rev. B* **2006**, *74* (22), 224421. (k) Bałanda, M.; Tomkowicz, Z.; Haase, W.; Rams, M. *J. Phys.* **2010**, *303*, 1. (l) Vallejo, J.; Cano, J.; Castro, I.; Julve, M.; Lloret, F.; Fabelo, O.; Canadillas-Delgado, L.; Pardo, E. *Chem. Commun.* **2012**, *48* (62), 7726−7728. (m) Bernot, K.; Luzon, J.; Caneschi, A.; Gatteschi, D.; Sessoli, R.; Bogani, L.; Vindigni, A.; Rettori, A.; Pini, M. G. *Phys. Rev. B* **2009**, *79* (13), 134419. (n) Gregoli, L.; Danieli, C.; Barra, A.-L.; Neugebauer, P.; Pellegrino, G.; Poneti, G.; Sessoli, R.; Cornia, A. *Chem.—Eur. J.* **2009**, *15* (26), 6456−6467.

(3) (a) Fu, A.; Huang, X.; Li, J.; Yuen, T.; Lin, C. L. *Chem.—Eur. J.* **2002**, *8*, 2239−2247. (b) Manson, J. L.; Arif, A. M.; Miller, J. S. *Chem. Commun.* **1999**, *16*, 1479−1480. (c) Abu-Youssef, M. A. M.; Langer, V.; Luneau, D.; Shams, E.; Goher, M. A. S.; Öhrström, L. *Eur. J. Inorg. Chem.* **2008**, *2008* (1), 112−118. (d) Li, X.-B.; Ma, Y.; Zhang, X.-M.; Zhang, J.-Y.; Gao, E.-Q. *Eur. J. Inorg. Chem.* **2011**, *2011* (30), 4738−4744. (e) Li, R.-Y.; Wang, B.-W.; Wang, X.-Y.; Wang, X.-T.; Wang, Z.-M.; Gao, S. *Inorg. Chem.* **2009**, *48* (15), 7174−7180. (f) Jia, Q.-X.; Tian, H.; Zhang, J.-Y.; Gao, E.-Q. *Chem.—Eur. J.* **2011**, *17* (3), 1040−1051. (g) Abu-Youssef, M. A. M.; Mautner, F. A.; Vicente, R. *Inorg. Chem* **2007**, *46* (11), 4654−4659. (h) Zeng, M.-H.; Zhou, Y.-L.; Zhang, W.-X.; Du, M.; Sun, H.-L. *Cryst. Growth Des.* **2009**, *10* (1), 20−24. (i) Wang, X.-Y.; Wang, L.; Wang, Z.-M.; Su, G.; Gao, S. *Chem. Mater.* **2005**, *17* (25), 6369−6380. (j) Zhang, X.-M.; Wang, Y.-Q.; Li, X.-B.; Gao, E.-Q. *Dalton Trans.* **2012**, *41* (7), 2026−2033. (k) Zhao, J.-P.; Zhao, R.; Yang, Q.; Song, W.-C.; Hu, B.-W.; Zhang, X.-F.; Bu, X.-H. *Dalton Trans.* **2012**, *41* (16), 4852−4858. (l) Adams, C. J.; Muñoz, M. C.; Waddington, R. E.; Real, J. A. *Inorg. Chem.* **2011**, *50* (21), 10633−10642.

(4) (a) Näther, C.; Greve, J. *J. Solid State Chem.* **2003**, *176* (1), 259−265. (b) Wriedt, M.; Jess, I.; Näther, C. *Eur. J. Inorg. Chem.* **2009**, *10*, 1406−1413. (c) Wriedt, M.; Näther, C. *Dalton Trans.* **2009**, *46*, 10192−10198. (d) Wriedt, M.; Näther, C. *Eur. J. Inorg. Chem.* **2010**, *20*, 3201−3211. (e) Wriedt, M.; Näther, C. *Chem. Commun.* **2010**, *46* (26), 4707−4709. (f) Wriedt, M.; Sellmer, S.; Näther, C. *Inorg. Chem.* **2009**, *48* (14), 6896−6903. (g) Wriedt, M.; Sellmer, S.; Näther, C. *Dalton Trans.* **2009**, *38*, 7975−7984.

(5) (a) Boeckmann, J.; Näther, C. *Dalton Trans.* **2010**, *39* (45), 11019−11026. (b) Boeckmann, J.; Näther, C. *Polyhedron* **2012**, *31*, 587−595. (c) Boeckmann, J.; Näther, C. *Chem. Commun.* **2011**, *47* (25), 7104−7106.

(6) Foner, S.; Frankel, R. B.; McNiff, J. E. J.; Reiff, W. M.; Little, B. F.; Long, G. J. *AIP Conf. Proc.* **1975**, *24* (1), 363−364.

(7) Boeckmann, J.; Wriedt, M.; Näther, C. *Chem.—Eur. J.* **2012**, *18* (17), 5284−5289.

(8) Wöhlert, S.; Boeckmann, J.; Wriedt, M.; Näther, C. *Angew. Chem., Int. Ed.* **2011**, *50* (30), 6920−6923.

(9) Nakashima, S.; Yamamoto, A.; Asada, Y.; Koga, N.; Okuda, T. *Inorg. Chim. Acta* **2005**, *358* (2), 257−264.

(10) (a) Schröder, C.; Klingelhöfer, G.; Tremel, W. *Planet. Space Sci.* **2004**, *52* (11), 997−1010. (b) Schröder, C.; Bailey, B.; Klingelhöfer, G.; Staudigel, H. *Planet. Space Sci.* **2006**, *54* (15), 1622−1634.

(11) (a) Pohl, K.; Wieghardt, K.; Nuber, B.; Weiss, J. *J. Chem. Soc., Dalton Trans.* **1987**, *1*, 187−192. (b) Wöhlert, S.; Jess, I.; Näther, C. *Acta Crystallogr.* **2011**, *E67*, m1503. (c) Wöhlert, S.; Wriedt, M.; Jess, I.; Näther, C. *Acta Crystallogr.* **2010**, *66* (10), 1256.

(12) (a) Miyasaka, H.; Saitoh, A.; Yamashita, M.; Clerac, R. *Dalton Trans.* **2008**, *18*, 2422−2427. (b) Miyasaka, H.; Takayama, K.; Saitoh, A.; Furukawa, S.; Yamashita, M.; Clérac, R. *Chem.—Eur. J.* **2010**, *16* (12), 3656−3662.

(13) Morrish, A. H. *The Physical Principles of Magnetism*; Wiley: New York, 1966.

(14) Carlin, R. L.; Van Duyneveldt, A. J. *Acc. Chem. Res.* **1980**, *13* (7), 231−236.

(15) (a) Starr, C.; Bitter, F.; Kaufmann, A. R. *Phys. Rev.* **1940**, *58* (11), 977−983. (b) Groenendijk, H. A.; Blöte, H. W. J.; van Duyneveldt, A. J.; Gaura, R. M.; Landee, C. P.; Willett, R. D. *Physica B* **1981**, *106* (1), 47−58. (c) Hoogerbeets, R.; Wiegers, S. A. J.; Van Duyneveldt, A. J.; Willett, R. D.; Geiser, U. *Physica B* **1984**, *125* (2), 135−149. (d) de Jongh, L. L.; Miedema, A. R. *Adv. Phys.* **1974**, *23*, 1.

(16) Chaudhuri, P.; Oder, K.; Wieghardt, K.; Gehring, S.; Haase, W.; Nuber, B.; Weiss, J. *J. Am. Chem. Soc.* **1988**, *110* (11), 3657−3658.

(17) Ostrovsky, S.; Haase, W.; Drillon, M.; Panissod, P. *Phys. Rev. B* **2001**, *64* (13), 134418.

(18) (a) Narath, A. *J. Phys. Soc. Jpn.* **1964**, *19*, 2244−2245. (b) van der Bilt, A.; van Duyneveldt, A. J. *Physica B* **1978**, *95* (3), 305−316. (c) Narath, A. *Phys. Rev.* **1965**, *139* (4A), A1221−A1227. (d) Narath, A. *Phys. Lett. B* **1964**, *13* (1), 12−13.

(19) Foner, S.; Frankel, R. B.; Reiff, W. M.; Wong, H.; Long, G. J. *J. Chem. Phys.* **1978**, *68*, 4781−4783.

(20) Sheldrick, G. M. *Acta Crystallogr.* **2008**, *A64*, 112−122.

(21) *X-Area, Version 1.44, Program Package for Single Crystal Measurements*; STOE & CIE GmbH: Darmstadt, Germany, 2008.